Simultaneous Measurements of Local Axial and Radial Momentum Fluxes near a Radial Wall of a Helicon Source

Takeharu SUGAWARA, Kazunori TAKAHASHI and Akira ANDO

Department of Electrical Engineering, Tohoku University, Sendai 980-8579, Japan

Axial and radial momentum fluxes near a lateral wall in a helicon plasma source are preliminarily investigated by installing a momentum vector measurement instrument, which has a detector plate mounted on a double-pendulum structure movable in both the axial and radial directions. The result demonstrates the presence of the axial momentum flux transferred to the radial wall, which seems to be delivered by the ions having the axial velocity and lost to the wall. Furthermore, a significantly greater radial momentum flux is lost to the radial wall, implying that the energy loss occurs at the radial wall. The presently shown technique would be useful for identifying the spatial profile of the momentum vector of the plasma.

The momentum flux of plasmas is one of the crucial physical quantities associated with acceleration, transport, and confinement of various plasmas [1–4], since many of the plasma characteristics are well described by momentum equations, which imply that the external forces applied to fluids are balanced to their momentum flux. Therefore, the momentum balance is very often used to model various plasmas ranging from naturally occurring plasmas to artificially-made terrestrial plasmas in small laboratories.

One of the direct applications of the plasma momentum flux is an electric propulsion for spacecrafts [5]. The performance of the propulsion devices can be typically characterized by a thrust-to-power ratio F/P, a specific impulse I_{sp}, and a thruster efficiency η_p, where F and P are the thrust and the electric power, respectively [6]. The latter two are defined as

$$I_{sp} = \frac{F}{m_{dot}g}, \quad \eta_p = \frac{F^2}{2m_{dot}P},\qquad(1)$$

where m_{dot} and g are the mass flow rate of the propellant and the gravitational acceleration at sea level, respectively. Since all of the assessment parameters are given by the thrust F and the well-controlled parameters such as the electric power P and the mass flow rate m_{dot}, the measurement of the thrust F should be taken on top priority to assess the thruster performance in laboratories.

According to a momentum conservation of the spacecraft and the exhausted propellant, the thrust force is equal in magnitude and opposite in direction to the momentum flux exhausted from the spacecraft as well known as a rocket equation [6]. Therefore, the direct measurement of the thrust is indeed equivalent to the identification of the absolute value of the total momentum flux of the plasma;

being also useful for understanding other plasmas if the local momentum flux can be identified.

The direct and individual measurements of the total thrust and thrust components exerted to the axial wall, the radial wall, and the magnetic nozzle have clarified many aspects of physics in a magnetic nozzle helicon plasma thruster [7–15]. In highly ionized conditions, e.g., for propellants of xenon and krypton, or for several kW rf power in argon, the axially negative force on the radial wall, which directs to the downstream side and is integrated over the whole inner surface, has been detected in the individual measurement of the axial force onto the radial wall [15,16], while the models have assumed that the ions near the wall are axially slow and do not deliver their axial momentum to the wall [17–19]. This unexpected axial force to the radial wall has been interpreted as that the axially accelerated ions are lost to the radial wall; an axially asymmetric plasma density profile having an upstream density peak enhances the negative force, where a neutral depletion phenomenon induces the asymmetric density profile [20]. Subsequent particle-in-cell simulation for the small scale thruster has given the profile of the local axial momentum lost to the radial wall [21], which has not been performed in the laboratory experiment. Furthermore, the total force measurement onto the radial wall can not give the radial momentum flux to the wall in the axisymmetric configuration.

Here the direct and simultaneous measurements of the axial and radial momentum fluxes lost to the radial wall are performed in a helicon source by locating the detector plate near the radial wall, which is mounted on a double pendulum structure movable in the radial and axial directions. The results show that the significant radial momentum is lost to the radial wall and the loss of the axial momentum

author's e-mail: kazunori@ecei.tohoku.ac.jp

to the radial wall is also confirmed.

The simultaneous measurements of the axial and radial momentum fluxes to the detector plate are performed by a momentum vector measurement instrument (MVMI) shown in the previous bench test [22] and the schematic is shown in Fig. 1. It should be mentioned that the whole structure of the MVMI in the previous bench test is flipped; yielding more stabilized axial pendulum motion than the previous test. Very briefly, the momentum detector plate having the detecting area of 2 cm × 3 cm is mounted on a rotational arm attached to a pivot, which is further mounted on the axially movable pendulum stage. The detector plate has a surface directing the radially inward direction and exposed to the plasmas, while the back side of the plate and the arm are covered by an insulator structure and a glass tube, respectively, to minimize the force by the plasma exerted on the structure except for the detector surface. Furthermore, the structure of the dual pendulum is covered by a metallic grounded structure for shielding the rf signal and the plasma impinging the balance. When the ions having the radial ($m_i u_r$) and axial ($m_i u_z$) momentums impinge on the detector plate with their radial flux of $n_s u_r$, both the radial and axial forces are exerted to the plate; causing the radial and axial displacements of the pendulums. By measuring both the displacements in the radial and axial directions, the forces can be obtained with multiplying calibration coefficients relating the displacements to the forces. The previous bench test has shown the force resolutions close to 10 μN in both the directions. The calibration coefficients can be obtained by slowly sweeping the current supplied to the calibration coils, where the displacements and the forces imparted to the pendulums are simultaneously measured by light-emitting-diode (LED) sensors and the load cells to which permanent magnets (PMs) are attached, respectively, being very similar to the procedure of a large-diameter target pendulum in Ref. [23]. This procedure can be done in vacuum in the present configuration by connecting all the electric signals and the coil current

via vacuum feedthroughs. Furthermore, the experiment in Ref. [23] has shown the excellent agreement between the directly measured thrust and the force to the target. Since the energy range of the incident ions is similar to and the target material is same as those in Ref. [23], the measurement reported here is considered to be reliable.

Figure 2 (a) shows the schematic diagram of the experimental setup. A helicon source consisting of a 100-mm-diameter pyrex glass source tube wound by a double-turn rf loop antenna at $z = -150$ mm and a solenoid locating at $z = -62$ mm is attached to a 600-mm-diameter and 1400-mm-long diffusion chamber evacuated by a turbomolecular pumping system to a base pressure of about 10^{-4} Pa, where $z = 0$ is defined as the open source exit. A dc solenoid current I_B is supplied to the solenoid to form an axial magnetic field in the source and an expanding magnetic field in the diffusion chamber. Argon gas is continuously introduced from the upstream flange of the source via a mass flow controller and the flow rate is chosen as 20 sccm; then the argon pressure measured at the chamber sideport is about
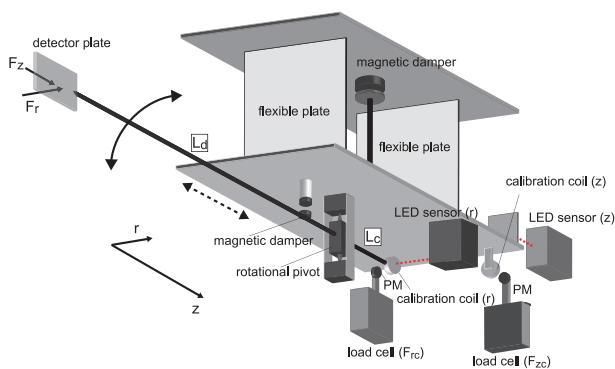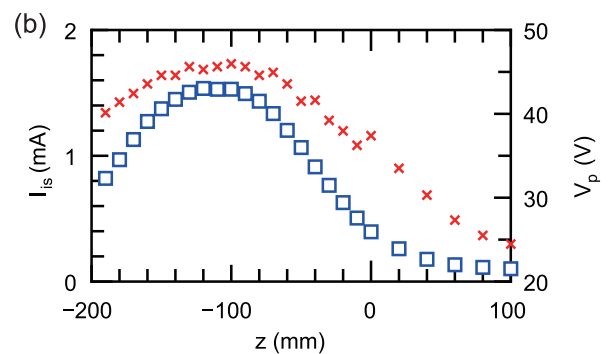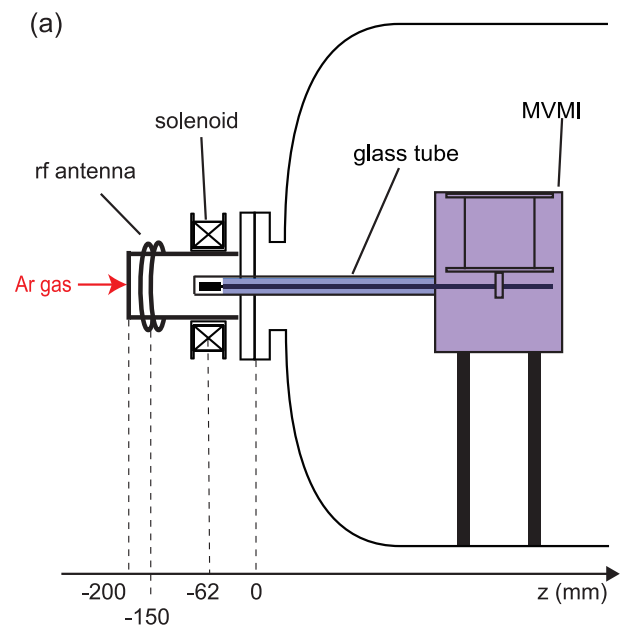

Fig. 1 Schematic diagram of the momentum vector measurement instrument (MVMI), where the whole structure is flipped from the previous bench test [22].

Fig. 2 (a) Schematic diagram of the experimental setup. (b) Measured ion saturation current I_{is} (open squares) and the local plasma potential V_p (crosses) on axis.

0.7 Pa. The solenoid current is chosen as 5 A here, providing the magnetic field of ~100 Gauss at the solenoid center. The antenna is powered by a 13.56 MHz rf generator via an impedance matching circuit. The forward rf power from the generator is set as 400 W and the variable capacitors in the matching circuit is tuned so as to minimize the reflected power, being typically less than a Watt.

Under the above-described condition, the axial profile of an ion saturation current I_{is} of a 3-mm-diameter planar Langmuir probe is taken on axis as plotted by open squares in Fig. 2 (b). When assuming the ion saturation current is given by $I_{is} = 0.61 e n_p u_B S$ with the elementary charge e, the plasma density n_p, the Bohm velocity u_B, and the collecting area S, the plasma density for $I_{is} \sim 1.5$ mA [corresponding to the maximum in Fig. 2 (b)] is estimated as about $(6.8 \pm 0.5) \times 10^{17}$ m^{-3} for the electron temperature of $T_e = 4.2 \pm 0.6$ eV, which is measured by a Langmuir probe assuming a Maxwellian energy distribution. The axial profile is fairly uniform inside the source as observed in the previous measurement of the electron energy probability function [24]. The profile shows that the maximum density position is about $z \sim -120$ mm.

The MVMI is immersed in the vacuum as seen in Fig. 2 (a) and the location of the detector plate is set at $z = -60$ mm and $r \sim 4$ cm being close to the radial source wall. This axial location corresponds to the downstream side of the maximum plasma density, where the plasma potential V_p has a maximum value as plotted by crosses in Fig. 2 (b). Since the electric field and pressure gradient toward the source exit is present between the maximum density position of $z \sim -120$ mm and the open source exit ($z = 0$), the presence of the axially accelerated ions toward the source exit at the MVMI detector position can be expected.

Figure 3 shows the voltage signals (V_r, V_z) from the LED sensors and the force signals (F_{rc}, F_{zc}) from the load cells when sweeping the (a) radial and (b) axial calibration coil currents, respectively, where the measured data are plotted by dots. The results show good linearly and can be fitted by linear lines as drawn by the bold solid lines in Fig. 3. The relation between the forces and the displacement signals are also described as the inset texts in Fig. 3. It has to be mentioned that the radial displacement is actually induced by a torque rather than the force. Therefore the radial force to the detector plate can be related with the displacement signal by multiplying the factor of L_c/L_d to the coefficient in Fig. 3 (a), where L_c (= 70 mm) and L_d (= 375 mm) are the arm lengths from the pivot to the calibration coil and to the detector plate, respectively. In the present experiment, the relations between the forces (F_r, F_z) to the detector and the displacement signals (V_r, V_z) can be given as

$$F_r = \frac{L_c}{L_d} F_{rc} = 0.889 V_r, \qquad (2)$$

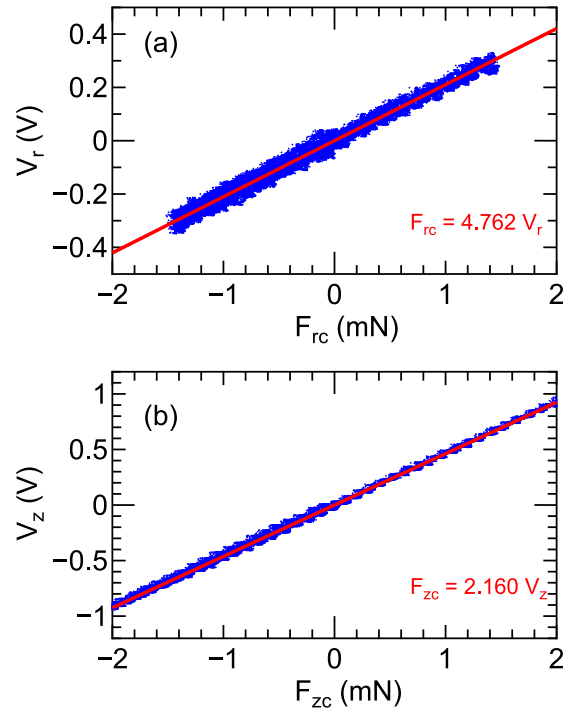$$F_z = F_{zc} = 2.160 V_z, \qquad (3)$$

Fig. 3 The measured forces and the displacement sensor signals (dots) when sweeping the currents of the (a) radial and (b) axial calibration coils. The bold solid lines show the fitted linear lines giving the calibration coefficients shown by the inset texts in Fig. 3.

where (F_r, F_z) and (V_r, V_z) are in units of mN and V, respectively. It is noted that the errors in these calibration coefficients are about 3 - 4% as reported before [22].

Thin lines in Fig. 4 show the displacement signals simultaneously measured by the two LED sensors for the radial and axial force measurements, where the solenoid current $I_B = 5$ A and the rf power for the plasma production are turn on for $t \sim 10$ - 40 sec and for $t \sim 20$ - 30 sec, respectively. Since both the radial and axial pendulum motions include the oscillation frequencies close to 2 Hz, being inherent to the restoring force of the pendulum, the data are filtered by using a Fourier transform and the filtered signals are plotted by the bold solid line. The displacement induced by only the solenoid current (at $t \sim 10$ and 40 sec) originates from a magnetic force somewhere, e.g., exerted on SUS304 metallic parts or the permanent magnets for the magnetic damper. The force exerted by the plasma can be obtained from the difference in the signal between 'RF on' and 'RF off' as analyzed in Ref. [25]. It should be mentioned that the positive change in V_r and V_z correspond to the forces in the radially outward and axially downward directions. From the positive change in both the V_r and V_z for the plasma production at $t \sim 20$ - 30 sec, it can be deduced that the radially outward and axially downward momentum fluxes are lost to the radial source wall. The absolute values of the fluxes of the radial and axial momentums (or forces) to the 2 cm × 3 cm detec-
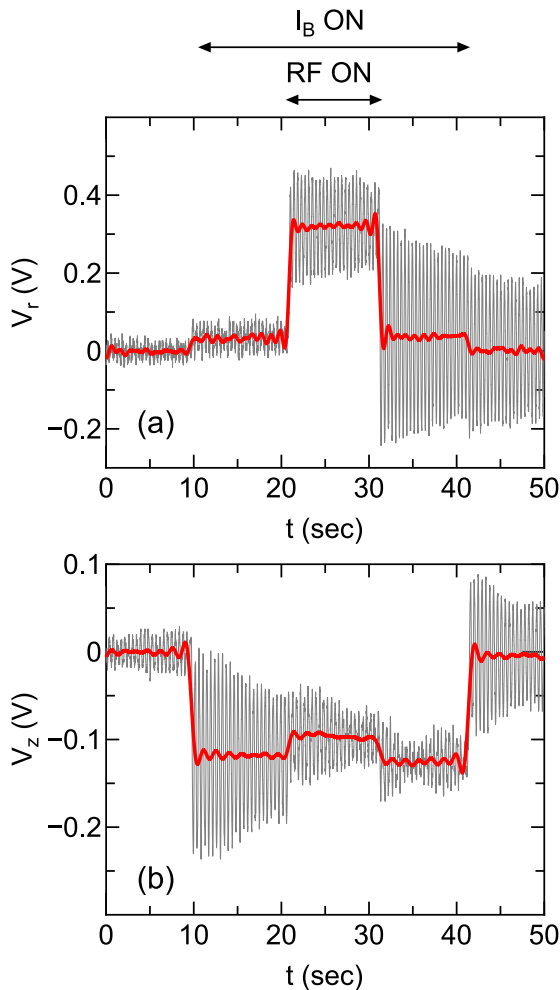
Fig. 4 The LED displacement sensor signals in the (a) radial and (b) axial directions, where the solenoid current I_B and the rf power are turned on for $t \sim 10$ - $40\,\text{sec}$ and for $t \sim 20$ - $30\,\text{sec}$, respectively. The positive changes of the signals indicate that the radially outward and axially downstream forces are exerted to the detector plate.

tial profiles of the radial and axial momentum fluxes will be obtained, which still remains an experimental challenge. The MVMI technique will also be useful for identifying characteristics of a high energy ion beam such as the beam emittance and the divergence.

tor plate are about 0.255 mN and 0.058 mN, respectively, corresponding to the force densities of about $0.425\,\text{N/m}^2$ and $0.1\,\text{N/m}^2$. The result demonstrates the significant loss of the radial momentum and the presence of the axial momentum transferred to the radial source wall, where the large radial momentum flux is expected to result from the radial ion acceleration in the sheath.

In summary, the momentum vector measurement instrument (MVMI) is installed near the radial wall of the helicon plasma source attached to the diffusion chamber. The simultaneous measurements of the radial and axial momentum fluxes lost to the detector plate are demonstrated here; implying the significant loss of the radial momentum flux and the presence of the axial momentum flux transferred to the radial source wall. By mounting the MVMI on the movable stage inside the vacuum chamber, the spa-

[1] D.L. Meier, S. Koide and Y. Uchida, Science **291**, 84 (2001).
[2] T.E. Eastman, Geophys. Res. Lett. **3**, 685 (1976).
[3] A.G. Peeters, C. Angioni and D. Strintzi, Phys. Rev. Lett. **98**, 265003 (2007).
[4] K. Takahashi, Rev. Mod. Plasma Phys. **3**, 3 (2019).
[5] S. Mazouffre, Plasma Sources Sci. Technol. **25**, 033002 (2016).
[6] D.M. Goebel and I. Katz, *Fundamentals of Electric Propulsion* (A John Wiley and Sons, Inc., Hoboken, 2008) chap. 2.
[7] K. Takahashi, T. Lafleur, C. Charles, P. Alexander, R.W. Boswell, M. Perren, R. Laine, S. Pottinger, V. Lappas, T. Harle and D. Lamprou, Appl. Phys. Lett. **98**, 141503 (2011).
[8] S. Pottinger, V. Lappas, C. Charles and R. Boswell, J. Phys. D: Appl. Phys. **44**, 235201 (2011).
[9] K. Takahashi, T. Lafleur, C. Charles, P. Alexander and R.W. Boswell, Phys. Rev. Lett. **107**, 235001 (2011).
[10] C. Charles, K. Takahashi and R.W. Boswell, Appl. Phys. Lett. **100**, 113504 (2012).
[11] A. Shabshelowitz and A. Gallimore, J. Propul. Power **29**, 919 (2013).
[12] L.T. Williams and M.L.R. Walker, J. Propul. Power **29**, 520 (2013).
[13] T. Harle, S.J. Pottinger and V.J. Lappas, Plasma Sources Sci. Technol. **22**, 015015 (2013).
[14] K. Takahashi, C. Charles and R.W. Boswell, Phys. Rev. Lett. **110**, 195003 (2013).
[15] K. Takahashi, A. Chiba, A. Komuro and A. Ando, Phys. Rev. Lett. **114**, 195001 (2015).
[16] K. Takahashi and A. Ando, Plasma Phys. Control. Fusion **59**, 054007 (2017).
[17] A. Fruchtman, IEEE Trans. Plasma Sci. **36**, 403 (2008).
[18] E. Ahedo and J. Navarro-Cavallé, Phys. Plasmas **20**, 043512 (2013).
[19] T. Lafleur, Phys. Plasmas **21**, 043507 (2014).
[20] K. Takahashi, Y. Takao and A. Ando, Appl. Phys. Lett. **108**, 074103 (2016).
[21] Y. Takao and K. Takahashi, Phys. Plasmas **22**, 113509 (2015).
[22] K. Takahashi, T. Sugawara, H. Akahoshi, Y. Takao and A. Ando, AIP Adv. **8**, 105117 (2018).
[23] K. Takahashi, A. Komuro and A. Ando, Rev. Sci. Instrum. **86**, 023505 (2015).
[24] K. Takahashi, C. Charles, R.W. Boswell, T. Kaneko and A. Ando, Phys. Plasmas **14**, 114503 (2007).
[25] K. Takahashi, C. Charles, R.W. Boswell and A. Ando, Plasma Sources Sci. Technol. **23**, 044004 (2014).